Journal of Materials Science and Engineering A 14 (1-3) (2024) 26-33
doi: 10.17265/2161-6213/2023.1-3.004

Investigating Stability Properties for Transition Metal Carbonate Precursors Using Universal Cluster Expansion Technique (UNCLE) as Cathodes for Li-Ion Batteries

M. T. Morukuladi[1], N. L. Lethole[2], M. C. Masedi[1], N. N. Ngoepe[1] and P. E. Ngoepe[1]

1. Materials Modelling Centre, University of Limpopo, Private Bag x1106, Sovenga 0727, South Africa

2. Department of Physics, University of Fort Hare, Alice 5700, South Africa

Abstract: The universal cluster expansion technique was used in this study to determine the binary phase diagrams for the transition metal carbonate precursors MCO_3 (M: Mn, Ni, Co). The use of mixed cathode materials in lithium-ion batteries such as NMC (Ni, Mn and Co) formulations, is a strategic approach to optimize performance, enhance safety and address cost and environmental considerations in the rapidly evolving field of energy storage. This study focuses on the cost issue related to lithium ion batteries by investigating the manganese rich NMC since manganese is more abundant and cost-effective. We doped $MnCO_3$ with nickel and doped $MnCO_3$ with cobalt then ran cluster expansion calculations to generate binary phases. The binary phase diagrams generated indicated that doping $MnCO_3$ with nickel favours the Mn-rich side, while doping $MnCO_3$ with cobalt favours 50% Mn-rich and 50% Co-rich. We further extracted the most stable structures from both binary diagrams and determined their electronic, mechanical and vibrational stabilities using DFT (density functional theory) calculations within the LDA (local gradient approximation) with Hubbard parameter (U). The electronic properties revealed that both materials are semiconductors due to their narrow energy band gap obtained while the mechanical properties showed that structures are mechanically stable since their necessary conditions for trigonal and triclinic systems were satisfied.

Key words: Binary phase diagrams, mechanical properties, electronic conductivity, phonon dispersion curves.

1. Introduction

To fully incorporate energy storage components into the grid and transportation sectors, the next-generation cathode materials for LIBs (lithium-ion batteries) needs to be developed. Cathode material is one of the four components within the LIB, which is most crucial in the application potential for LIBs. To provide strong battery performance, such as rate capability and cycling performance, cathode materials with different compositions and crystal structures should have the structural robustness [1-3]. Cathode materials have attracted researcher's attention due to their various chemistries available in the market, to enhance LIB's performance [4, 5]. Among various cathode materials already in the market, $LiCoO_2$ (lithium cobalt oxide) has been the most widely used and commercialised cathode material [6] for LIBs, however this material was found to be toxic, very expensive and exhibiting low theoretical capacity of 140 mAh/g when it is cycled between 3 V and 4.2 V, hindering the widespread application in LIBs [7].

As a result of the drawbacks discovered by this well-studied cathode material, there has been an extensive quest for researchers to find cathode materials with high volumetric density and high specific reversible discharge capacity for application in LIBs. As such, the

Corresponding author: Mogahabo Tebogo Morukuladi, Ph.D., Ms., research fields: materials science.

transition metal oxides commonly referred to as NMC's were found as the most dominant and alternative cathodes in today's LIBs due to their inherent safety, low cost and high capacity of >250 mAh/g as compared to $LiCoO_2$ with the capacity of ~140 mAh/g [8-10]. Lithium and manganese-rich composites are strongly recommended as sustainable alternatives for the next generation of cathode materials [11] due to the synergistic effect of nickel, manganese, and cobalt. Moreover, $LiNi_xMn_yCo_zO_2$ is one of the most successful combinations of nickel-manganese-cobalt as a new generation energy storage material, providing very good performance in terms of specific power, life span, cost, safety, and excels in specific energy. The combination of nickel, manganese, and cobalt allows for a balance between specific energy (energy density) and power capability. Nickel provides high specific energy, while cobalt enhances power performance. Manganese contributes to achieving a balance between the two, optimizing the overall performance of the battery [12]. Therefore, combining these elements enhances each other's strengths leading to overall better performance of the electrode material.

The objectives of this study were to generate binary phase diagrams ($NiMnCO_3$ and $CoMnCO_3$) and to understand the stability properties for most stable phases using first principle calculations. This paper focuses on investigating the binary structural properties to understand their behaviours before moving to ternary investigations. We computationally doped manganese carbonate with nickel and cobalt to determine their stability properties. We then used the UNCLE code to generate their binary phase diagrams and predict the most stable strutures from the figures and calculate their structural, electronic and mechanical properties using first principles calculations.

2. Methodology

The universal cluster expansion (UNCLE) technique, developed by Hart et al. [13] was utilised in this study to generate the binary phase diagrams of the transition metal carbonate structures. The UNCLE code applies a genetic algorithm to find the best possible set of clusters, each of which has interaction parameters that are based on the energies of the structures in a training set. It further calculates the total energy of systems for various configurations of these clusters using more accurate quantum mechanical methods such as the DFT (density functional theory). During the CE (cluster expansion) fitting process, the effective structures are iteratively added to the training set and when CE finds no additional ground state structures, convergence is then reached. From the generated binary phase diagrams, most stable phases were explored by determining their stability properties using first principle calculations employing the DFT with PAW (projector augmented wave) [14] pseudopotential, in VASP [15] code within MedeA software. The number of planewaves was determined using a kinetic cut-off energy of 500 eV and the Brillouin zone sampling scheme of Monkhorst-pack with 4×4×4 *k*-points mesh for all the transition metal carbonate structures. The elastic properties were calculated using a strain of 0.003, while the DOSs (densities of states) were calculated for both spin-up and spin-down in the spin-polarized magnetism.

3. Results and Discussions

3.1 Binary Phase Diagrams

Binary phase diagrams are graphical representations that show the relationships between the phases of two components in a binary system at equilibrium, typically as a function of energy of formation and concentration. They are also crucial in predicting the ordered or disordered superstructures of systems. The binary ground state diagram summarises the generation of new structures and prediction of formation of the structures considered by cluster expansion. Fig. 1 presents the binary ground state diagram of $NiMnCO_3$ while Fig. 2 presents the ground state diagram of $CoMnCO_3$. The

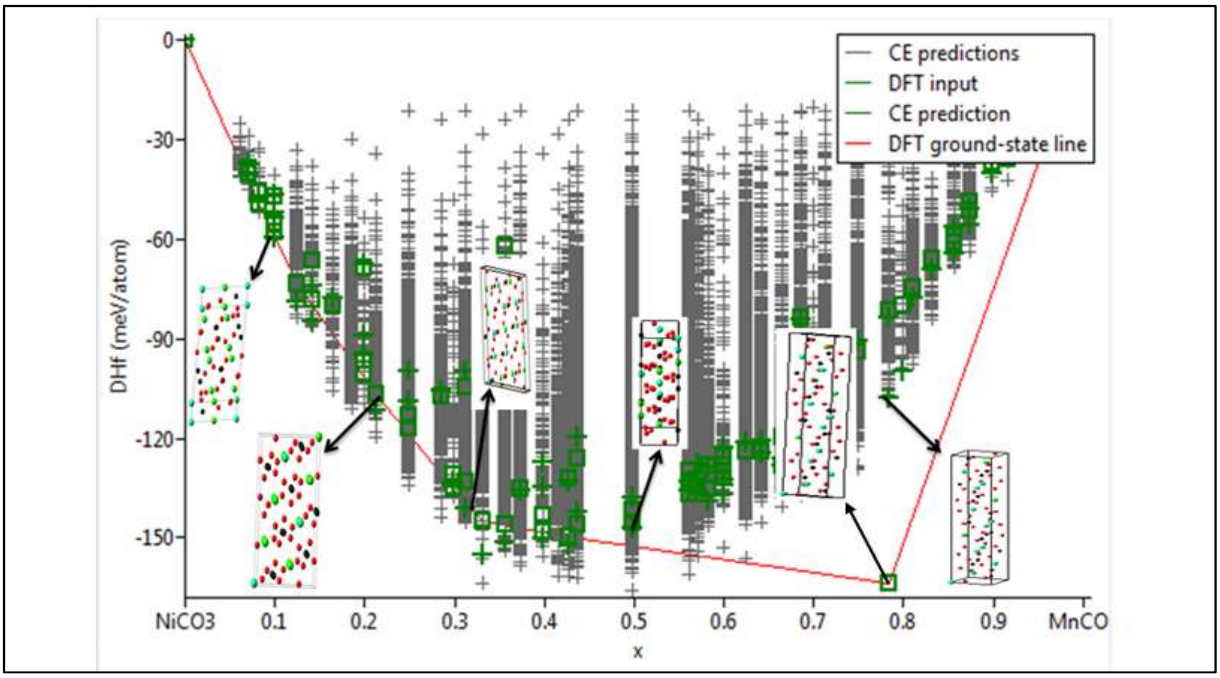

Fig. 1 Binary phase diagram for $NiMnCO_3$.

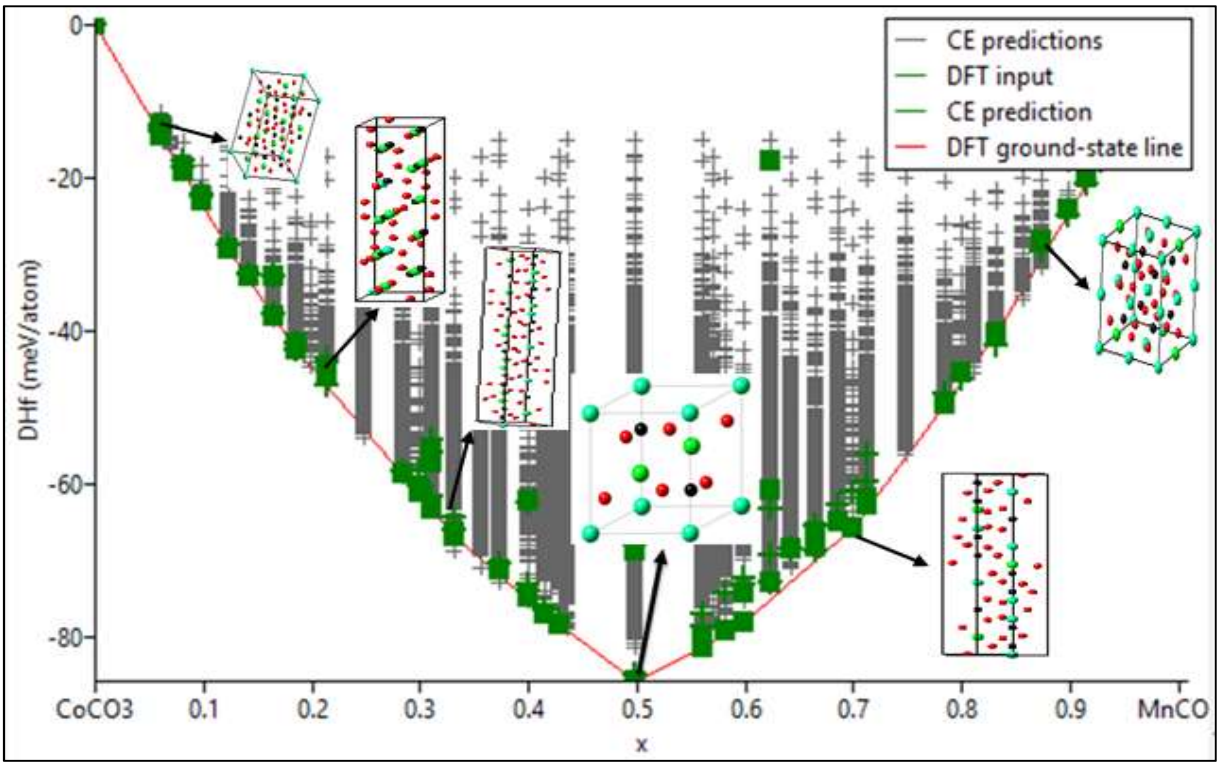

Fig. 2 Binary phase diagram for $CoMnCO_3$.

red line that appears within the phase diagrams forms the convex hull connected by ground state structures. The convex hull represents the absolute lowest formation energy that can be achieved during the whole composition range. From the figures, we note that the grey CE prediction entries represent the structure space within which the ground state structures are identified, while the red CE entries represent the

training set structures, for which DFT energies are calculated.

Figs. 1 and 2 show that all the phases generated are in the negative heats of formation which implies that generated phases are thermodynamically stable (miscible constituent). We further note that doping $MnCO_3$ with Ni favours the Mn rich side, while doping $MnCO_3$ with Co favours 50% Co and 50% Mn. This indicates that for $NiMnCO_3$, the structure at $x = 0.8$ ($Ni_{0.2}Mn_{0.8}CO_3$) is the most stable as compared to other compositions due to its least energy of formation. On the other hand, in Fig. 2 we note that $Mn_{0.5}Co_{0.5}CO_3$ is the most stable structure with $x = 0.5$. Both diagrams show the miscible constituent behaviour, which indicate that structures are ordered, hence thermodynamically stable. We also note that some CE enumerated structures are slightly below the convex hull. These are spurious ground states that lie within the numerical errors of the fitting process for CE coefficients. Moreover, the green squares that are shown within phase diagrams represent structures which are most favourable within a bcc-type lattice phases, which were predicted as ground state structures in the cluster expansion run.

3.2 DOS

We have determined the DOS to understand the electronic properties of $Ni_{0.2}Mn_{0.8}CO_3$ and $Mn_{0.5}Co_{0.5}CO_3$, by calculating their spin polarised total and partial DOS as shown in Figs. 3a and 3b. The DOS for structures can be used to check the stability trend with respect to their behaviour at the Fermi level (E_f). The total electronic contribution of a whole system is indicated by the total DOS while the contribution of each individual atom is indicated by the partial DOS.

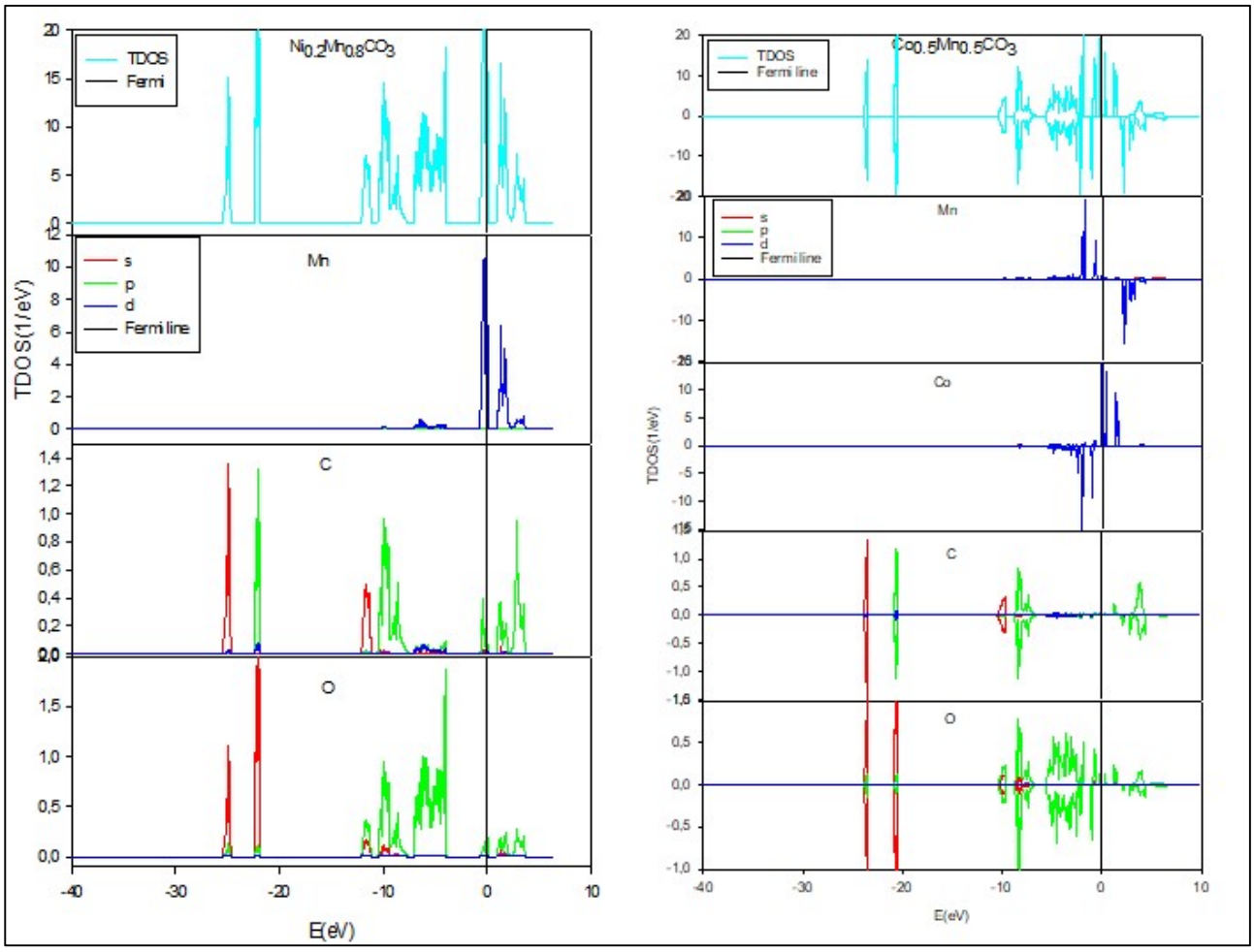

Fig. 3 DOS for (a) $Ni_{0.2}Mn_{0.8}CO_3$ and (b) $Co_{0.5}Mn_{0.5}CO_3$.

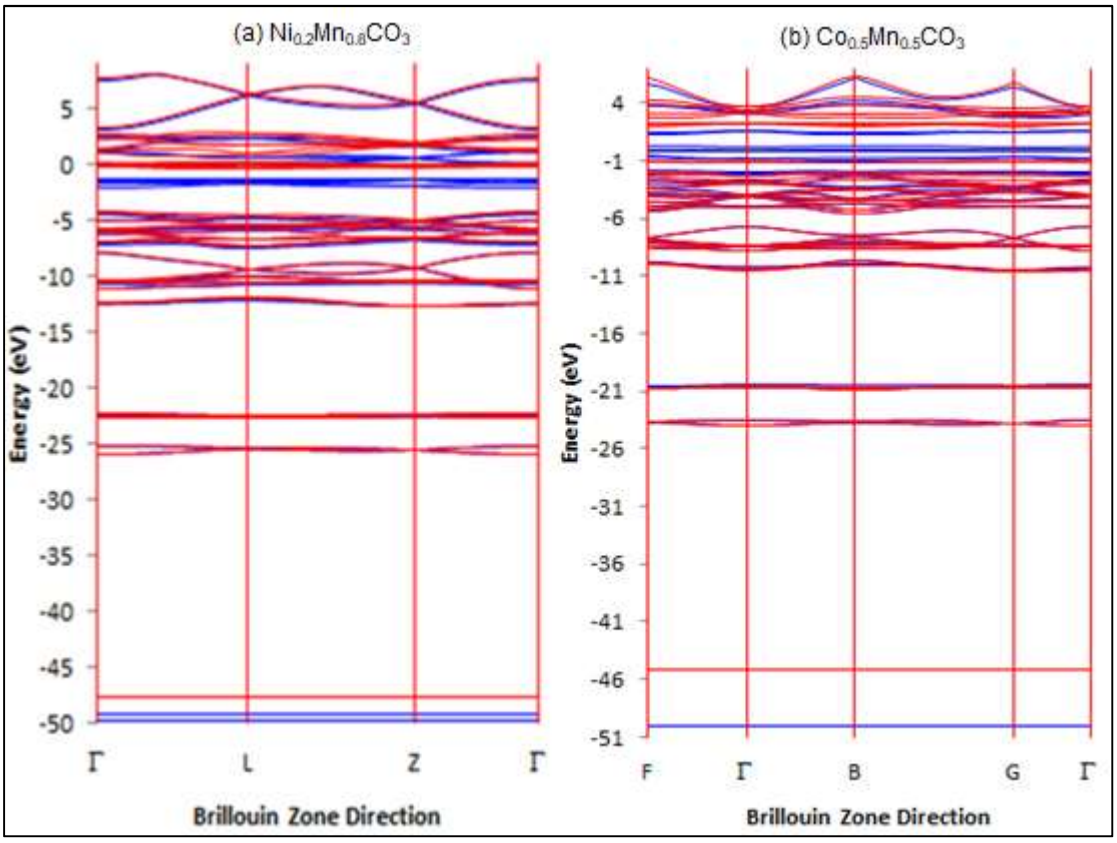

Fig. 4 Electronic band structures for (a) $Ni_{0.2}Mn_{0.8}CO_3$ and (b) $Co_{0.5}Mn_{0.5}CO_3$.

For $Ni_{0.2}Mn_{0.8}CO_3$, we note that the fermi level is located on the edge of the valence band with an indirect band gap of 0.211 eV suggesting a semiconductor behaviour. The partial DOS plots indicate that the states in the energy range of -10 eV to 0 eV are predominately of oxygen p-states and manganese p-states. $Co_{0.5}Mn_{0.5}CO_3$ plot as shown in Fig. 3b shows that the fermi level is located on the edge of the valence band. However, we note an indirect energy band gap of 0.229 eV, suggesting that the material is a semiconductor. Hence, both phases are good electronic conductors with the stability trend as follows:

$$Ni_{0.2}Mn_{0.8}CO_3 > Co_{0.5}Mn_{0.5}CO_3 \quad (1)$$

3.3 Band Structures

To determine the electronic properties for $Ni_{0.2}Mn_{0.8}CO_3$ and $Mn_{0.5}Co_{0.5}CO_3$, we have calculated their energy band structures along high symmetry directions. Band structures give information about the conductivity of materials. As shown in Fig. 4, we note that both systems have an indirect energy band gaps of 0.211 eV and 0.229 eV which implies that our systems are magnetic semiconductors. However, in literature review we found that the band structures for $MnCO_3$ and $CoCO_3$ were 3.53 eV and 2.64 eV [16]. So our results prove that indeed mixing these elements together improves their stability behaviour due to the narrow energy band gaps obtained for $Ni_{0.2}Mn_{0.8}CO_3$ and $Mn_{0.5}Co_{0.5}CO_3$ respectively.

3.4 Elastic Properties

From the binary phase diagrams we wanted to understand the mechanical properties for the most stable phases by determining their elastic properties. The elastic constants were calculated using Taylor expansion of total energy given by:

$$U(V,\varepsilon) = U(V_0,0) + V_0\left[\sum_i \tau_i\varepsilon_i,\delta_i + \frac{1}{2}\sum_{ij} C_{ij}\tau_i\varepsilon_i,\delta_i\right] \quad (2)$$

where $U(V_0, 0)$ is the energy of the unstrained system with equilibrium volume V_0, τ_i is an element in the stress tensor and δ_i is a factor to take care of Voigt index. After the calculations, we found that elastic constants for $Ni_{0.2}Mn_{0.8}CO_3$ falls within the trigonal crystal lattice as it contained six independent elastic constants ($C_{11}, C_{12}, C_{13}, C_{14}, C_{33}, C_{44}$). So for trigonal crystal lattices to be considered mechanically stable, the following necessary mechanical stability conditions must be satisfied [17];

$$C_{11} - |C_{12}| > 0, (C_{44} + C_{12})C_{33} - 2C_{13}^2 > 0, (C_{11} + C_{12})C_{44} - 2C_{14}^2 > 0 \quad (3)$$

As shown in Table 1, we note that our LDA+U calculated elastic constants satisfy the mechanical stability conditions for trigonal systems, indicating mechanical stability. From the calculated elastic constants, the macroscopic bulk (B), shear (G) and Young's (E) moduli were estimated using the Voigt-Ruess-Hill approximation method [18-20] as shown in Table 2. Our calculated Bulk and Young moduli results were found to be high and positive, indicating hardness or stiffness respectively. To determine the brittleness and ductility nature for the structure, we have calculated the B/G ratio as proposed by Pugh [21]. Materials are considered ductile if the B/G ratio value is greater than 1.75, otherwise they are considered brittle. We note that our calculated B/G ratio value is less than 1.75 indicating brittleness.

Contrary to $Ni_{0.2}Mn_{0.8}CO_3$, the elastic constants for $Co_{0.5}Mn_{0.5}CO_3$ were found to contain 21 independent elastic constants, which implies that the material falls within the triclinic lattice criterion. For triclinic systems to be considered mechanically stable, the following necessary and sufficient born stability conditions must be satisfied [22, 23].

$$C_{11} > 0, C_{22} > 0, C_{33} > 0, C_{44} > 0, C_{55} > 0, C_{66} > 0 \quad (4)$$

Hence, $Co_{0.5}Mn_{0.5}CO_3$ material was found to be stable as it satisfied all the mechanical stability conditions for triclinic systems. We also note that our calculated B/G ratio value for $Co_{0.5}Mn_{0.5}CO_3$ is greater than 1.75 which indicates that the material is ductile.

Table 1 Elastic constants for most stable structures.

	$Ni_{0.2}Mn_{0.8}CO_3$	$Co_{0.5}Mn_{0.5}CO_3$
C_{11}	359.36	190.45
C_{12}	83.20	89.90
C_{13}	88.64	54.79
C_{14}	29.30	-4.42
C_{15}	-	4.56
C_{16}	-	-1.18
C_{22}	-	197.83
C_{23}	-	56.67
C_{24}	-	7.13
C_{25}	0.00	-5.06
C_{26}	-	-1.66
C_{33}	178.92	117.42
C_{34}	-	1.23
C_{35}	-	-0.29
C_{36}	-	1.62
C_{44}	100.26	36.45
C_{45}	-	-0.08
C_{46}	-	-4.51
C_{55}	-	35.63
C_{56}	-	-4.33
C_{66}	-	50.00

Table 2 Calculated Moduli and Pugh ratios for $Ni_{0.2}Mn_{0.8}CO_3$ and $Co_{0.5}Mn_{0.5}CO_3$.

(GPa)	$Ni_{0.2}Mn_{0.8}CO_3$	$Co_{0.5}Mn_{0.5}CO_3$
B	151.79	96.28
G	103.10	43.26
E	252.21	112.87
$\frac{B}{G}$	1.47	2.26

4. Conclusions

We successfully used the universal cluster expansion technique to mix the transition metal carbonate precursors. Cluster expansion methods were utilised in this study to generate stable phases from binary phase diagrams. The generated binary phase diagrams showed that mixing $NiMnCO_3$ results in miscible constituent, which indicates that all structures generated are thermodynamically stable and ordered as they are all in the negative energy of formation. However, the most stable structure was found at the Mn-rich side as this structure had the least energy of

formation. Similar to $NiMnCO_3$, the binary phase diagram revealed that all generated structures are thermodynamically stable and ordered as they fall within the negative energy of formation. The most stable structure was found to appear at 50% Co-rich and 50% Mn-rich. We further sought to analyse the electronic conductivity of $Ni_{0.2}Mn_{0.8}CO_3$ and $Co_{0.5}Mn_{0.5}CO_3$ by determining their DOS and band structures. The results revealed that both materials are semiconductors due to the narrow energy band gap recorded. This is an indication that both phases are good electronic conductors. The calculated elastic constants for $Ni_{0.2}Mn_{0.8}CO_3$ and $Co_{0.5}Mn_{0.5}CO_3$ suggested mechanical stability, since they satisfied the necessary born stability criterion for trigonal and triclinic crystals. Our results indicate that $Ni_{0.2}Mn_{0.8}CO_3$ performs better than $Co_{0.5}Mn_{0.5}CO_3$ in most of the stability properties investigated.

The continuation of this study will be to add minor amount of cobalt on $Ni_{0.2}Mn_{0.8}CO_3$ material forming a ternary phase and investigate their stability properties for possible applications as cathodes for lithium ion batteries.

Acknowledgements

This work was performed at MMC (Materials Modelling Centre) of the University of Limpopo and the CHPC (Centre for High Performance Computing) with the support of the South African Research Chair Initiative of the Department of Science and Technology is greatly appreciated. The study was funded by the NRF (National Research Foundation) with grant number 128934, and this funding is really appreciated.

References

[1] Malik, M., Chan, K., and Azimi, G. 2022. "Review on the Synthesis of $LiNi_xMn_yCo_{1-x-y}O_2$ (NMC) Cathodes for Lithium-Ion Batteries." *Materials Today Energy* 28: 101066.

[2] Yabuuchi, N., and Ohzuku, T. 2005. "Electrochemical Behaviors of $LiCo_{1/3}Ni_{1/3}Mn_{1/3}O_2$ in Lithium Batteries at Elevated Temperatures." *Journal of Power Sources* 146: 636-9.

[3] Venkateswara Rao, C., Leela Mohana Reddy, A., Ishikawa, Y., and Ajayan, P. M. 2011. "$LiNi_{1/3}Co_{1/3}Mn_{1/3}O_2$-Graphene Composite as a Promising Cathode for Lithium-Ion Batteries." *ACS Applied Materials and Interfaces* 3: 2966-72.

[4] Thackeray, M. M., Johnson, C. S., Vaughey, J. T., and Hackney, S. A. 2005. "Advances in Manganese-Oxide 'Composite' Electrodes for Lithium Ion Batteries." *Journal of Materials Chemistry* 23: 2257-67.

[5] Srivastava, N., Singh, S. K., Gupta, H., Meghnani, D., Mishra, R., Tiwari, R. K., Patel, A., Tiwari, A., and Singh, R. K. 2020. "Electrochemical Performance of Li-Rich NMC Cathode Material Using Ionic Liquid Based Blend Polymer Electrolyte for Rechargeable Li-Ion Batteries." *Journal of Alloys and Compounds* 843: 155615.

[6] Jiang, K. C., Xin, S., Lee, J. S., Kim, J., Xiao, X. L., and Guo, Y. G. 2012. "Improved Kinetics of $LiNi_{1/3}Mn_{1/3}Co_{1/3}O_2$ Cathode Material through Reduced Graphene Oxide Networks." *Physical Chemistry Chemical Physics* 14: 2934-9.

[7] Yoshio, M., Brodd, R. J., and Kozawa, A. 2009. *Lithium Ion Batteries*. New York: Springer.

[8] Schmuch, R., Wagner, R., Hörpel, G., Placke, T., and Winter, M. 2018. "Performance and Cost of Materials for Lithium-Based Rechargeable Automotive Batteries." *Nature Energy* 3: 267-78.

[9] Myung, S. T., Maglia, F., Park, K. J., Yoon, C. S., Lamp, P., Kim, S. J., and Sun, Y. K. 2017. "Nickel-Rich Layered Cathode Materials for Automotive Lithium-Ion Batteries: Achievements and Perspectives." *ACS Energy Letters* 2: 196-223.

[10] Schipper, F., Erickson, E. M., Erk, C., Shin, J. Y., Chesneau, F. F., and Aurbach, D. 2016. "Review—Recent Advances and Remaining Challenges for Lithium Ion Battery Cathodes." *Journal of Electrochemichal Society* 164: 6220-8.

[11] Nitta, N., Wu, F., Lee, J. T., and Yushin, G. 2015. "Li-Ion Battery Materials: Present and Future." *Materials Today* 18: 252-64.

[12] Miao, Y., Hynan, P., Von Jouanne, A., and Yokochi, A. 2019. "Current Li-Ion Battery Technologies in Electric Vehicles and Opportunities for Advancements." *Journal of Energy Storage* 12: 1074.

[13] Hart, G. L. W., Muller, S. G., and Forcade, R. W. 2009. "UNCLE: A Code for Constructing Cluster Expansion for Arbitrary Lattices with Minimal User Input." *Modelling Simulation for Material Science Engineering* 17: 330-90.

[14] Blochi, P. E. 1994. "Projector Augmented Wave." *Physical Review* 50: 17953-79.

[15] Schimka, L., Harl, J., Stroppa, A., Grüneis, A., Marsman, M., Mittendorfer, F., and Kresse, G. 2010. "Accurate

Surface and Adsorption Energies from Many-Body Perturbation Theory." *Nature Mater* 9: 741-4.

[16] Morukuladi, M. T., Lethole, N. L., Masedi, M. C., Ngoepe, N. N., and Ngoepe, P. E. 2022. "Structural, Electronic, Elastic and Dynamical Properties of MCO_3 (M: Mn, Co, Ni) Precursor Materials for Li-Ion Batteries: A First Principles Study." *Journal of the Electrochemical Society* 169 (2): 2-7.

[17] Mei, H., Pang, Y., Yu, D., and Cheng, N. 2018. "Electronic and Mechanical Properties of Trigonal Boron Nitride by First-Principles Calculations." *Physica E: Low-Dimensional Systems and Nanostructures* 101: 16-21.

[18] Hill, R. 1952. "The Elastic Behaviour of a Crystalline Aggregate." *Proceedings of the Physical Society, Section A* 65: 349-55.

[19] Reuss, A., and Angew, Z. 1929. "Calculation of the Flow Limits of Mixed Crystals on the Basis of the Plasticity of Monocrystals." *Zeitschrift fur Angewandte Mathematik und Mechanik* 9: 49-58.

[20] Voigt, W. 1928. "Lehrbuch der Kristallpysik Taubner." *Leipzig* 213: 29-35.

[21] Pugh, S. F. 1954. "Relations between Elastic Moduli and the Plastic Properties of Polycrystalline Pure Metals." *The Philosophical Magazine* 45: 823-43.

[22] Mouhat, F., and Coudert, F. X. 2014. "Necessary and Sufficient Elastic Stability Conditions in Various Crystal Systems." *Physical Review* 90: 224104-34405.

[23] Kantorovich, L. 2014. *Quantum Theory of the Solid State: An Introduction.* London: Kluwer Academic Publishers, pp. 10244-01.